Radiometry at infrared wavelengths for agricultural applications

Thomas J. Schmugge, W.P. Kustas

Agronomie 19 (1999) 83–96

Review article

Radiometry at infrared wavelengths for agricultural applications

Thomas J. Schmugge*, W.P. Kustas

USDA/ARS Hydrology Lab, Bldg 007, BARC-West, Beltsville, MD 20705-2350, USA

(Received 23 November 1998; accepted 9 February 1999)

Abstract – Measurements of thermal radiation at infrared wavelengths (7–14 μm) yield much information about the land surface. The primary use of these observations is for surface temperature determination as the emissivity is usually close to one. For this purpose it is fortuitous that the peak in the thermal emission occurs in an atmospheric transmission window. In additions there are variations in the emissivity of minerals and soils in the 7–14-μm region which can be interpreted for identification purposes. The emissivity for vegetative canopies has been found to be close to one with little spectral variation. Applications of the derived surface temperature to study the surface energy balance and to estimate the energy fluxes from the land surface are discussed. The basic concepts of the energy balance at the land surface are presented along with an example of how remotely sensed surface brightness temperatures can be used to estimate the sensible heat and to estimate plant water use. The example is from the Monsoon 90 experiment conducted over an arid watershed in the state of Arizona in the United States. In this case, surface temperatures derived from an aircraft thermal infrared sensor and vegetation and land use characteristics derived from a Landsat TM image were used in a two-source model to predict the surface heat fluxes. The agreement with ground measurements is reasonably good for the 3 days of observations. (© Inra/Elsevier, Paris.)

remote sensing / thermal infrared / surface fluxes

Résumé – Applications agricoles de la radiométrie infrarouge. Les mesures de radiation thermique aux longueurs d'ondes infrarouges (7 à 14 μm) fournissent une riche information concernant la surface des terres. Ces observations sont utilisées en premier lieu pour déterminer la température de surface, puisque l'émissivité en est généralement proche. Dans ce cas il arrive par hasard que le pic dans l'émission thermique se trouve dans la fenêtre de transmission atmosphérique. En outre il y a des variations de l'émissivité des minéraux et des sols dans la bande 7 à 14 μm, qui peuvent être interprétées dans des buts d'identification. On a trouvé que l'émissivité des canopées de la végétation était proche de la valeur un, avec une petite variation spectrale. On discute des applications de la température de surface dérivée à l'étude de l'équilibre énergétique de surface et à l'estimation des flux d'énergie envoyé par la surface des terres. Les concepts de base de l'équilibre énergétique à la surface des terres sont présentés avec un exemple qui montre comment les

Communicated by Gérard Guyot (Avignon, France)

* Correspondence and reprints
schmugge@hydrolab.arsusda.gov

températures de brillance de surface télédétectées peuvent être utilisées pour estimer la chaleur sensible et l'utilisation de l'eau par la plante. L'exemple est tiré de l'expérience Mousson 90 qui a été faite au-dessus d'une ligne de partage des eaux en région aride, dans l'état d'Arizona. Dans ce cas, les températures de surface provenant du détecteur infrarouge thermique de l'avion et les caractéristiques de la végétation et de l'utilisation des terres provenant de l'image Landsat TM ont été utilisées dans un modèle à deux sources pour prédire les flux de chaleur de surface. Les résultats concordent assez bien avec les mesures de terrain faites durant les trois jours d'observation.

télédétection / infrarouge thermique / flux de surface

1. INTRODUCTION

Measurement of the thermally emitted radiation at various wavelengths from the earth's surface can yield much useful information about parameters such as surface soil moisture and temperature. These two parameters are very important for the study of the land–atmosphere interaction. The partitioning of the net radiation into latent and sensible heating components is determined by the moisture available in the soil for the evapotranspiration process. The value of the surface temperature is the result of this partitioning. If sufficient moisture is available the surface temperature will be close to that of the air. If not the surface temperature will rise above that of the air and contribute more strongly to the sensible heat flux.

To estimate surface temperatures, radiation at wavelengths around 10 mm is used because the peak intensity of the thermal emission occurs in this region for terrestrial temperatures (300 K) and in addition the atmosphere is relatively transparent and the observed variations in the intensity of radiation are mainly related to surface temperature. However, it must be kept in mind that variations in emissivity of 1 % yield brightness temperature variations of 0.3–0.6 K depending on sky radiance. To estimate surface soil moisture, radiation at much longer wavelengths (10s of cm) is used. Changes in the intensity of the emitted radiation at these wavelengths are primarily due to the variation of the emissivity with the moisture content of the soil. This effect results from the large dielectric contrast between water and dry soils. This topic has been discussed in an earlier paper by Wigneron et al. [50] in this journal.

The monitoring of the land surface fluxes at regional spatial scales is recognised as important for applications such as the modelling of atmospheric behaviour, the monitoring of water resources and the estimation of plant or crop water use [21]. Surface temperature is a key boundary condition for many land–surface atmosphere models, and a variable that can be measured by satellite remote sensing on a global basis. Indeed, considerable progress has been made in accounting for atmospheric effects and variation in surface emissivity so that the uncertainty in radiometric surface temperature measurements from satellites is within 1–2 degrees [30].

An example of a thermal infrared image from the airborne thermal infrared multispectral scanner (TIMS), obtained during the HAPEX-MOBILHY experiment conducted in southwestern France during June 1986 [1] is shown in *figure 1*. This image is of the central site area, which is a clearing in the Les Landes pine forest. It shows a mixture of agricultural fields, both bare and vegetated, and forests. When one looks at this image, it is obvious that the large variations in surface brightness temperatures, T_B, arise from differences in the surface energy balance for the different surfaces. Recall that T_B is a measure of the radiation emitted from the surface and is directly related to the temperature of the surface and its emissivity. In *figure 1* the hotter fields (white, with $T_B \approx$ 40–50 °C) are either bare soil or fields with sparse, newly emerging vegetation. The cooler fields (black, with $T_B \approx$ 25–30 °C) are completely vegetated or forested. These temperature contrasts among fields with different vegetation conditions imply a different partition of the incoming solar energy into latent and sensible heat components. In general, cooler temperatures indicate that there is sufficient moisture available so that

Figure 1. Thermal infrared image from channel 5 (10–11 μm) of TIMS acquired during the HAPEX-MOBILHY experiment in southwest France in 1986. The data were acquired at an altitude of 6 km with a pixel size of 15 m and cover an area of approximately 10 by 15 km. North is up in the figure. The range of temperature is from 30 °C for the well-watered vegetation fields and forests to almost 50 °C for the bare soil fields.

most of the incoming energy goes into latent heat or evaporation, while hotter temperatures indicate that most of the incoming energy goes into the sensible or convective heating of the atmosphere. This image also demonstrates another part of the problem of determining the surface fluxes which arises due to the differences in the aerodynamic properties (i.e. heat transfer coefficients) for the various types of vegetation and their heights, ranging from the 20-m pine forests to the 1- or 2-m vegetation in cropped fields which may have the same T_B values. The problem is to quantify these fluxes in terms of the remotely sensed T_B. There is a long history on the use of T_B to monitor these surface fluxes (e.g. [21, 34, 41, 44]) and in this paper we will describe the contributions remotely sensed thermal infrared data can make towards quantifying these fluxes.

2. THERMAL INFRARED RADIATION

The intensity of the thermal radiation from an object is described by the Planck black body relationship given as a function of frequency in equation (1a) and as a function of wavelength in equation (1b):

$$L_{BB}(\nu, T) = \frac{2\,h\,\nu^3 / c^2}{\exp(h\,\nu / k\,T) - 1} \qquad (1a)$$

$$L_{BB}(\lambda, T) = \frac{2\,h\,c^2 / \lambda^5}{\exp(h\,c\ / \lambda\,k\,T) - 1} \qquad (1b)$$

where h is Planck's constant (6.626×10^{-34} J s), c is the speed of light and k is Boltzmann's constant(1.381×10^{-23} J K^{-1}). The units are W m^{-2} sr^{-1} per Hz for equation (1a) or W m^{-2} sr^{-1} per meter for (1b). Equation (1a) is plotted in *figure 2* for several temperatures. In this figure the reflected solar radiation is also plotted for albedos of 0.1 and 1 to show that at the wavelengths where the terrestrial thermal radiation peaks, i.e. at $\lambda \approx 10$ μm, the reflected solar radiation is several orders of magnitude weaker. The wavelength for the maximum in the thermal emission curve is given by the Wien displacement law where $\lambda_{max} T \approx 2.898 \times 10^{-3}$ m K. Thus, for a temperature of 300 K, $\lambda_{max} \approx 9.7$ μm. Thus, measurements around this wavelength should yield information on surface temperature without any contamination by reflected solar radiation. The cosmic background radiation at $T = 3$ K is also shown for reference.

In the infrared we usually speak in terms of wavelength while in the microwave frequency and wavelength are used interchangeably. We think this results from the techniques used to quantify the waves: in the infrared wavelengths can be measured but not frequency while in the microwave both frequency and wavelength can be measured. It should

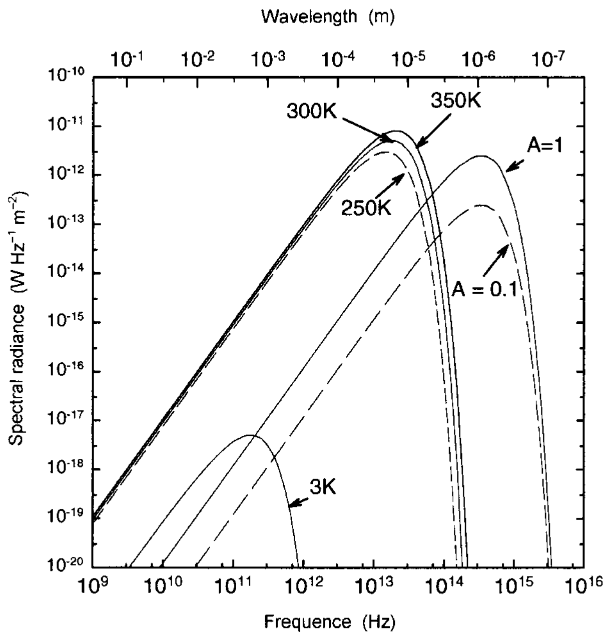

Figure 2. The spectral radiance of a black body according to equation (1a) for a typical range of terrestrial temperatures and the cosmic background (3 K). The reflected solar irradiance with indicated values of the albedo (α) is also plotted for comparison. Adapted from Schanda [42].

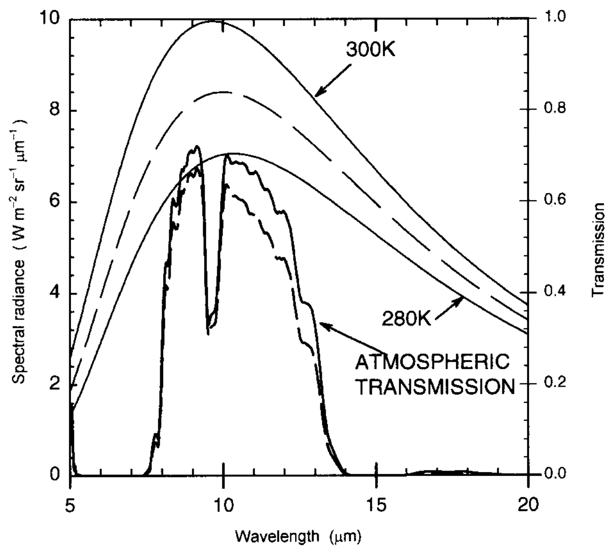

Figure 3. The spectral radiance of a black body according to equation (2) for typical terrestrial temperatures and the atmospheric transmission for the US Standard mid-latitude summer atmosphere with two moisture levels: the upper curve is for a columnar water content of 2.9 g cm^{-2} and the lower is for 3.5 g cm^{-2}.

be noted that in the infrared frequency is usually expressed in terms of wavenumber, i.e. $\nu = 1/\lambda$, in cm^{-1}. In this case equation (1a) is usually represented as

$$L_{BB}(\nu, T) = \frac{\varepsilon c_1 \nu^3}{\exp(C_2 \nu / T) - 1} \tag{2}$$

where C_l is 1.19104×10^{-8} W/(m^{-2} sr^{-1} cm^{-4}), C_2 is 1.4388 cm K and ν is expressed in wavenumber (cm^{-1}) ε and is the emissivity. For a perfect emitter or black body $\varepsilon = 1$, and for real surfaces $\varepsilon < 1$.

2.1. Atmospheric effects

In *figure 3*, we have plotted equation (2) from 5 to 20 μm for temperatures 280, 290 and 300 K, i.e. near the low range of terrestrial temperatures. At these temperatures the peak emission occurs in the 8–10-μm range of wavelength. In this figure we have also plotted the clear sky atmospheric transmission calculated with the Modtran4 path radiance model [7] for the mid-latitude summer atmosphere, assuming the radiometer is at satellite altitude. While the atmosphere is relatively transparent in the 8–12-μm range compared to adjacent wavelengths, there is still significant attenuation. As seen in *figure 3* there is only 60–70 % transmission with a major dip at about 9.5 μm due to ozone absorption. With the exception of this dip, water vapour is the dominant absorber in the 8–12-μm window. This is due mainly to what is called the water vapour continuum since only in the 8–9-μm range are there any relatively strong absorption lines. Thus, the magnitude of the atmospheric effect will depend on the water vapour content of the intervening atmosphere. The atmospheric transmission for a 20 % increase in water vapour is also plotted to indicate this sensitivity to water vapour. This unknown or uncertain atmospheric contribution is one of the problems for the remote sensing of surface temperature at infrared wavelengths. This, of course, is in addition to clouds which will totally obscure the surface at visible and infrared wavelengths.

The radiation values given in *figure 3* are those which would be observed right at the surface; the relation between the radiation, L_i, seen by a radiometer on a satellite or aircraft and the surface temperature is:

$$L_i = \left[\varepsilon_i \cdot L_{BB_i}(T) + \left(1 - \varepsilon_i\right) \cdot L_{atm_i}(dn)\right] \cdot \tau_i + L_{atm_i}(up) \quad (3)$$

where the subscript i indicates the integral of these quantities over the band width for channel i of the radiometer, L_{BBi} is the Planck function given by equation (1), the L'_{atm}s are the upward and downward components of the atmospheric radiation and τ is the atmospheric transmission. The values of L_{atm} and τ can be calculated using a model for atmospheric path radiance such as Modtran4; however, it would be preferable to eliminate the atmospheric effects using the multispectral information.

Several approaches have been developed for eliminating atmospheric effects in the estimation of sea surface temperature from space using multichannel thermal data. The technique used with the AVHRR (advanced very high resolution radiometer) data from the NOAA series of polar orbiting satellites involves the differential water vapour absorption in the 10–13-µm window with the 11.5–13-µm portion being more strongly absorbed, the so-called split window technique [17, 27]. However, this assumes that the surface emissivity is constant over this spectral band, which is not the case for land surfaces [5, 17]. There have been a number of recent papers on the use of split window techniques over land with the AVHRR data [6, 23, 49]. In order to better understand thermal infrared radiation we need to study the behaviour of the emissivity of terrestrial materials or surfaces.

2.2. Infrared emissivity

There has been much use of the spectral variation of infrared emissivities for geological purposes [2]; here we are more interested in the emissivities of soils and vegetation. This discussion will be based on recent papers by Salisbury and D'Aria [37, 38] which present emissivity spectra in the 8–12-µm range for soils and vegetation. These results were based on laboratory and field measurements made with an interferometer.

To extract the emissivity from the radiance measurements, the assumption is made that the emissivity is unity somewhere in the wave band observed. A blackbody curve is fitted to that portion of the spectra to obtain the temperature. The emissivity is then determined by dividing the observed radiance by the black body radiance at that temperature [22]. However, to do this with field measurements it is necessary to take into account the reflected sky radiation as indicated in *figure 4* where the true and apparent emissivity are plotted as functions of wavelength for a case with significant downwelling radiance. *Figure 4a* shows the downwelling atmospheric radiance calculated with Modtran4 for a tropical atmosphere with 4.2 g cm^{-2} of water vapour. The upper three curves show surface radiances; the top is for a black body at 300 K, the lowest of the three is for the emission from a quartz-rich sandy soil and the middle curve is the upwelling radiance at the surface, i.e. the term in brackets in equation (3) which includes the reflected downwelling radiance. When the latter two curves are divided by the blackbody curve the true and apparent emissivities are obtained as shown in lower portion of the figure. This example shows the importance of measuring the downwelling sky radiance in emittance measurements. Note that for the quartz sand shown here the emissivity is about 0.8 at $\lambda = 9.2$ µm.

An example of the emissivity variation of soils is given in *figure 5* where spectral variation for three soils from the US are presented. The soil data are from the Johns Hopkins Spectral Library Salisbury et al. [38]. They show the pronounced effect of quartz (SiO_2), gypsum and carbon on the emissivity spectra for the two soils with emissivity being less than 0.9 for $\lambda < 9.5$ µm for quartz or gypsum. Note that in the 10–12-µm range the emissivity is high, ~0.95, and relatively constant. The response functions for the six channels of the TIMS (thermal infrared multichannel scanner) radiometer are also shown.

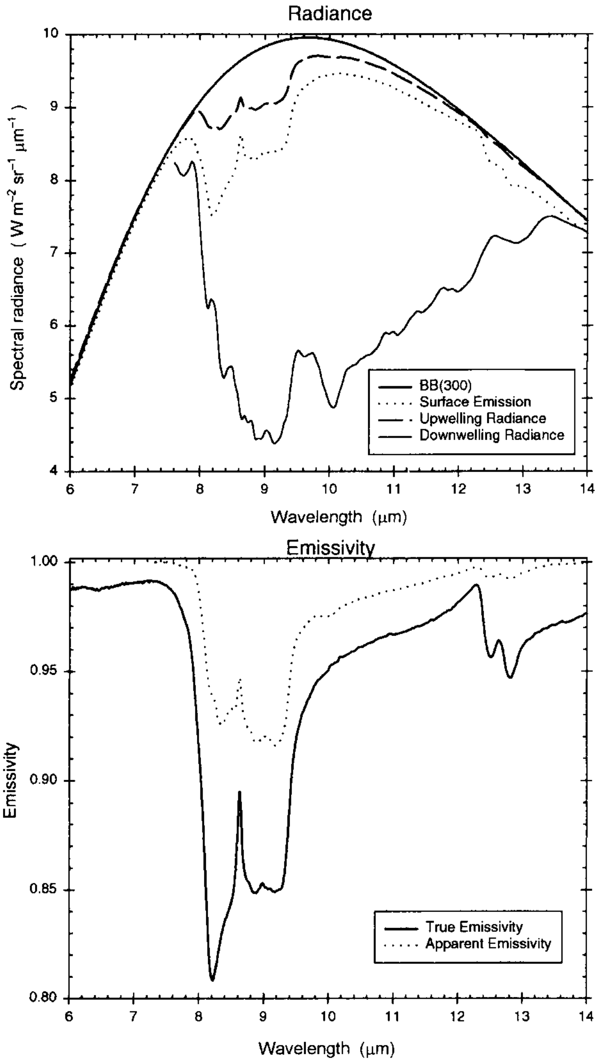

Figure 4. The effect of downwelling atmospheric radiance on apparent emissivity. Top: radiances; the surface radiance components to equation (3), the bottom curve is the downwelling radiance, the top curve is the blackbody radiance from equation (2), the curve below that is upwelling radiance at the surface, i.e. the term in brackets in equation (3) and final curve is the emission from the surface. Bottom: emissivity; the true and apparent emissivity.

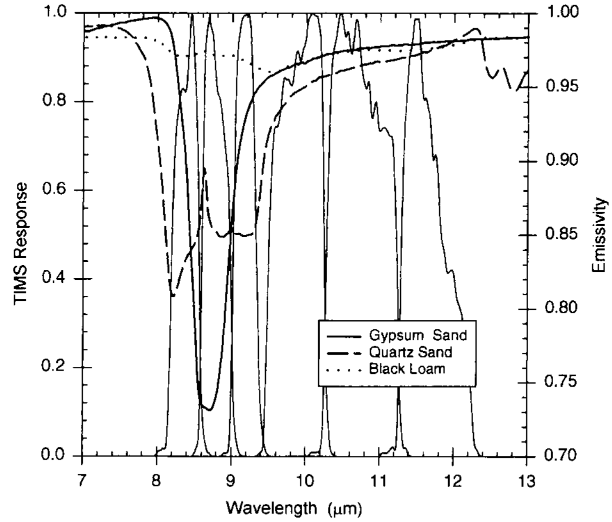

Figure 5. Laboratory measurements of the emissivity for three soils from the USA with the filter functions for the six TIMS channels. The soils are: 1) Brown sand with 0.5 % organic carbon, 2 % clay and 96 % quartz; 2) white gypsum dune sand with 0 % organic carbon, 0 % clay and 99 % gypsum with a trace of quartz; and 3) black loam with 6.6 % organic carbon, 30 % clay and 56 % quartz.

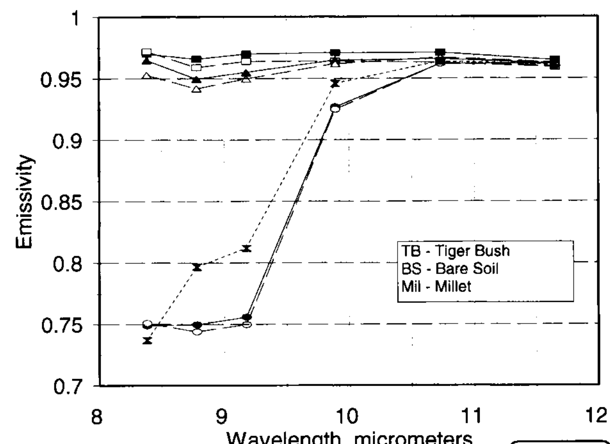

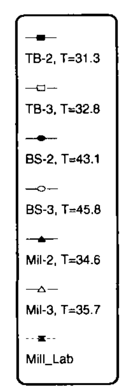

Figure 6. Aircraft emissivity values for a bare soil field and vegetated conditions from HAPEX-Sahel. The aircraft values are derived from data obtained with the TIMS sensor at an altitude of 1 500 m and are for two passes, open and closed symbols, at about 14:00 local time. The derived temperatures are given in the legend. The results from laboratory measurements are indicated with the hourglass symbol.

Emissivity values derived from TIMS data obtained on an aircraft platform during the HAPEX-Sahel experiment are shown in *figure 6* [39]. The emissivities were derived using the TES (temperature emissivity separation) algorithm developed for use with ASTER data from the EOS satellite [16]. The results from two passes over the target area are shown: the solid symbols are for the first and the open symbols are for the second pass 20 min later on 4 September 1992. There is excellent agreement between the two lines. Especially for the bare soil case, where the emissivities for channels 1, 2 and 3 ($8 < \lambda < 9.5$ µm) are about 0.75 in both lines. There is a slightly greater difference for the two vegetation targets especially for the millet field and for the shorter wavelength channels but for both these targets there is little spectral variation expected for a vegetation target. Note that there are slight differences in the derived temperatures for all three targets. The second pass was about 20 min later than the first and there was a 0.5 °C drop in air temperature over this interval, not enough to account for the 1–1.5 °C difference in the derived temperatures for the vegetation targets. However, for Tiger Bush the derived temperatures are within 1 °C of the air temperature. The bare soil results are in reasonable agreement with laboratory measurements for a sample from a millet field site indicated by the hourglass symbol. These measurements were made by the group at the University of Strasbourg [28]. These results indicate that it is possible to extract these emissivity variations with remotely sensed data.

Results for a large number of soils are given in the paper by Salisbury and D'Aria [38]. For almost all of their soils the emissivity in the 10–12-µm band is higher than in the 8–9.2-µm band. The effect of quartz on the soils' emissivity depends on particle size, with the effect being greater for coarser soils, i.e. those with larger particle sizes. Since soil organic matter is highly absorbing in the thermal infrared with a relatively flat spectrum it reduces the spectral contrast of the quartz restrahlen bands as seen in *figure 5* by comparing the results for the sand and loam soils, which had 96 and 56 % quartz, respectively. A similar but smaller effect arises from the presence of moisture in the soil because the flat absorption spectrum of water has the effect of increasing the emissivity in the 8–9.2-µm band for quartz-rich soils.

In addition to minerals and soils Salisbury and D'Aria [37] present spectra for a number of terrestrial materials. These include various vegetative components such as green and senescent foliage.

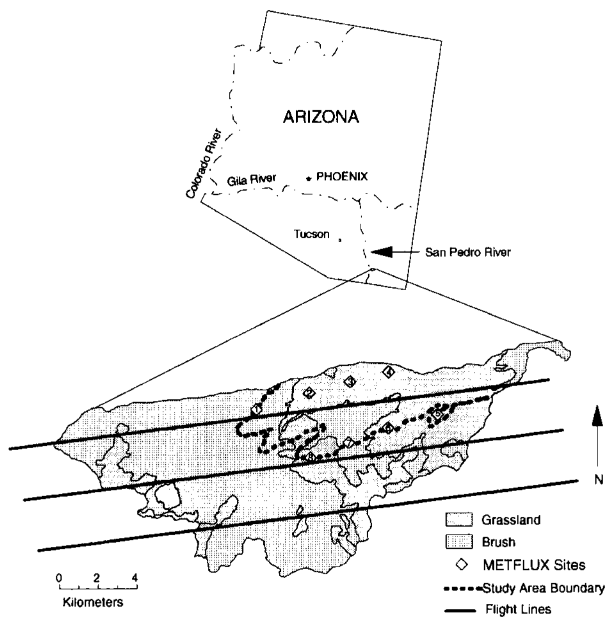

Figure 7. A schematic plan showing the location of the USDA-ARS Walnut Gulch experimental watershed with a map delineating the shrub and grass dominated ecosystems. The straight lines represent the flight lines flown by the NASA C-130 aircraft over the watershed during the Monsoon 90 field experiment. Data from only the upper two lines were used in this analysis. The approximate locations of the METFLUX sites are also shown.

For the green foliage the infrared reflectances are generally less than 5 %, emissivity > 0.95, while for senescent vegetation the reflectance is generally higher. As expected the soil litter has low reflectance. When these components are combined to form a vegetative canopy the results become more complicated because of scattering within the canopy. The net result is simpler because multiple scattering by the leaf surfaces with their low reflectance yields a canopy emissivity very close to one with little spectral variation. This was observed for the prairie grass in FIFE by Palluconi et al. [32], who found an emissivity of 0.99 ± 0.01, with no spectral variation. In HAPEX-MOBILHY Schmugge et al. [40] found little or no spectral variation over a coniferous forest or an oat field and over the Tiger Bush site in HAPEX-Sahel, see *figure 6*, using TIMS data from an aircraft platform. These results for vegetation are in substantial agreement with modeling studies of Norman et al. [29]

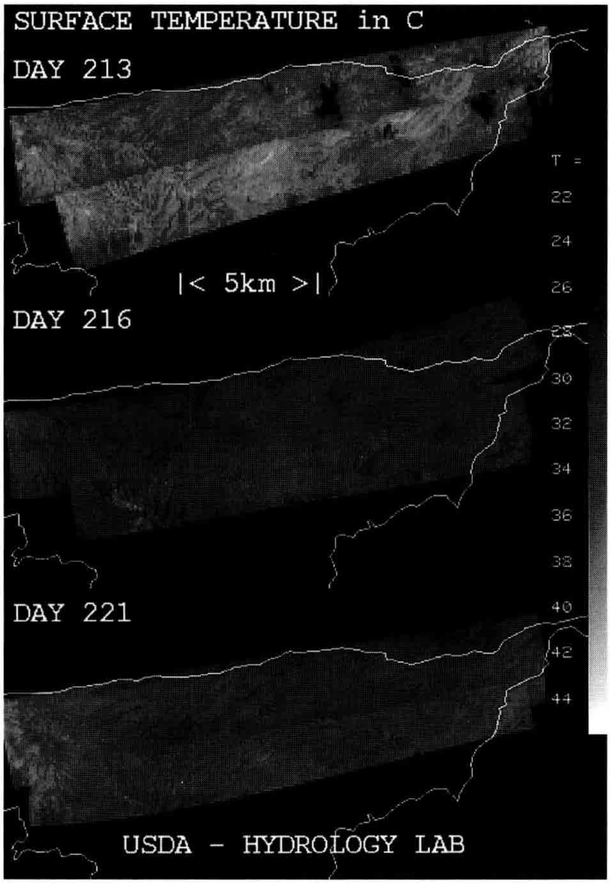

Figure 8. Surface brightness temperature maps for the Walnut Gulch watershed as part of the Monsoon 90 experiment. The data are from the thermal channel (#8) of the NS001 sensor from an altitude of 2 400 m on day 213 (1 August 1990), day 216 (4 August 1990), and day 221 (9 August 1990). Note the clouds on day 213.

who derived a value of 0.99 for the emissivity of the grass canopy in FIFE.

3. SURFACE FLUXES

3.1. Energy and moisture balance

To understand better how thermal infrared observations can contribute to the determination of the surface fluxes, let us consider the basic energy and moisture balance equations. In the absence of advection or precipitation the energy balance at the land surface is given by:

$$R_n - G - H - LE = 0 \tag{4}$$

where R_n is the net radiation, G the soil heat flux, H the sensible heat flux and LE the latent heat or moisture flux into the atmosphere. Here we are treating the heat fluxes (G, H and LE) away from the surface as being positive. The net radiation is the sum of the incoming and outgoing short- and long-wave radiation fluxes:

$$R_n = (1-\alpha)\cdot R_I + (1-\varepsilon)\cdot R_{L\downarrow} - \varepsilon\cdot\sigma\cdot T^4 \tag{5}$$

where α is the surface albedo, R_I is the incoming solar radiation, $R_{L\downarrow}$ is the incoming long-wave radiation, ε the surface emissivity and T the surface temperature in Kelvins.

There has been considerable progress in estimating R_I and α from geostationary satellite data. The basis of the method is that the major modulator of surface insolation is cloudiness. The information contained in the satellite radiances is interpreted in terms of scattering, reflection and absorption parameters which are subsequently used in radiative transfer model calculations for the atmosphere [15]. Dedieu et al. [14] give a description of the method applied to Meteosat data. They also estimate albedo α from these same data. $R_{L\downarrow}$ can be estimated from atmospheric sounders [8] or empirically from surface conditions [9]. The surface albedo can also be estimated from multi-spectral data [45]. So it would appear that the components of the radiation flux in equation (5) can be estimated reasonably well using remotely sensed data [47].

The difficulty arises then in determining the surface fluxes in equation (4). Both the sensible and ground heat flux involve temperature gradients: one in the soil and the other in the atmosphere. The latent heat flux involves the vapour pressure gradient. Thus, for the ground heat flux we have:

$$G = \lambda \frac{\partial T_{soil}}{\partial z} \tag{6}$$

where λ is the thermal conductivity of the soil. While the soil temperature gradient can not be determined from remotely sensed data, the temperature profile can be modelled with sufficient accuracy to estimate G. Also empirical data have shown that there is a reasonable relationship between the ratio G/R_n and vegetation indices such as the simple ratio (SR) and the normalised difference vegetation index (NDVI) [24].

The sensible heat flux into the atmosphere is:

(7)

where ρ is the air density, c_p is the specific heat of air at constant pressure, T_{aero} is the aerodynamic temperature in the canopy air space, T_a is the air temperature above the canopy and R_a is the aerodynamic resistance. The last term, R_a, is a rather complex function of various geometrical factors including roughness lengths, displacement heights and the wind speed, and is usually empirically determined. T_{aero} is the temperature of the source for the convective heat transfer and can be determined from the profiles of temperature and windspeed in the boundary layer [19]. For an aerodynamically smooth surface, T_{aero} and T_B, the radiometric brightness temperature, are equivalent since such a surface is the source for both the radiative and convective or sensible heat fluxes. This, of course, assumes an emissivity of 1. However, most natural surfaces are not smooth, and T_{aero} and T_B are not equivalent, as demonstrated by Hall et al. [18] working with data from FIFE. This difference between T_{aero} and T_B is thoroughly discussed by Norman et al. [30].

The latent heat flux is:

$$LE = \rho\, c_p \frac{(e_a - e_s)}{\gamma \bullet (R_a + R_s)} \qquad (8)$$

where γ is the psychrometric constant, e_a is the atmospheric vapour pressure in the boundary layer, e_s is the saturation vapour pressure at the temperature T_a and R_s is the stomatal resistance to water vapour transport. To get around the lack of knowledge of these temperature and vapour pressure gradients in the soil and lower atmosphere, 1-D models of the heat transfer in the soil and from the land surface into the atmosphere have been developed (e.g. [10, 11, 13, 43]). In particular Shuttleworth [43] gives a comprehensive review of evaporation models. These models use the remotely sensed surface temperature as a boundary condition and model parameters are varied to obtain the best fit between the predicted and observed surface temperatures [12, 48]. From equation (4), we see that available energy ($R_n - G$) is partitioned into latent and sensible heat components. The approach frequently used is to estimate H using the remotely sensed surface brightness temperature (T_B) in equation (7), and to determine LE as a remainder term.

Equation (7) implicitly assumes that the canopy is a thin layer with a single temperature, which is clearly not the case for a vertically developed canopy exhibiting variations in temperature. While both T_{aero} and T_B result from contributions of the surface temperatures of the canopy elements, they do so in different ways and as a result are not equivalent. The problem is that T_{aero} in equation (7), being the effective temperature for the canopy heat transfer process, is not a measurable quantity and is not equal to T_B, in general. If the classical value of R_a is used in equation (7) with T_B, Hall et al. [18] found poor agreement with observed fluxes. However, Stewart et al. [46] have shown that if an additional resistance term, R_r, is added for sparsely vegetated surfaces, the agreement improves substantially. Since T_B is generally larger than T_{aero} for partially vegetated surfaces resulting in a larger temperature gradient, an additional resistance term is necessary to maintain the same H. In addition, there is increased resistance to heat flow compared to that for the momentum flux for which R_a is derived.

The thermal radiation observed by a radiometer originates both from soil and from vegetation elements, which having various temperatures and orientations can lead to variations of T_B with viewing angle. This variation can be exploited to obtain more information about the canopy [31].

3.2. Examples of flux estimation

As noted in the previous section there are several problems for using the remotely sensed surface temperatures to estimate surface fluxes. These mainly involve the estimation of heat transfer coefficient between the surface and the atmosphere and the difference between the radiometric surface temperature and the temperature of the surface where the heat exchange takes place. In this section we will briefly present results from two approaches for solving these problems and estimating surface fluxes.

An approach which is applied on a pixel basis was developed by Bastiaanssen [3, 4, 33] called the surface energy balance algorithm for land (SEBAL). It requires observations in the visible, near-infrared and thermal infrared ranges to derive its needed parameters: surface albedo, vegetation index *NDVI* and surface temperature. The radiation components are derived by the methods described earlier in this paper, see equation (5). This approach makes use of an assumed relationship between the remotely sensed surface temperature and the air temperature and coupling this to the surface roughness for heat transport. The approach does require a limited number of ground measurements for calibration. The derived area averaged fluxes using LandSat TM data were in good agreement with results obtained in several recent large-scale field experiments including EFEDA (Spain, 1991), HAPEX-Sahel (Niger, 1992) and HEIFE (China).

An alternate approach requiring no calibration has been developed recently, which considers the contributions from the soil and canopy separately and which requires only a few additional parameters for implementation [31]. The surface energy balance is evaluated for each elemental area (defined by the pixel size of remotely sensed data), *i*, using the dual-source model. In this model the soil surface and vegetative canopy fluxes are considered in parallel with their own resistance to heat transfer. Norman et al. [31] also developed a series resistance network which is more complicated but may be more appropriate as it permits interaction between soil and vegetation. With these parallel paths, the sensible heat flux, equation (4), can be expressed as the sum of the contribution from the soil, H_S, and from the canopy, H_C, yielding the total flux by the following equation as a modification to equation (7):

$$H = H_C + H_S = \rho\, c_p \frac{(T_C - T_a)}{R_{AH}} + \frac{(T_S - T_a)}{(R_{AH} + R_S)} \qquad (9)$$

where R_S is the resistance to heat flow in the boundary layer immediately above the soil surface, R_{AH} is the resistance to heat transfer from the vegetated layer, T_a is the air temperature at a reference height in the atmosphere, and T_S and T_C are the soil and canopy temperatures, respectively.

Two assumptions are used to obtain a solution using equation (9) with the composite radiometric temperature of the surface, T_R. The first assumption is that T_R is related to canopy and soil temperatures, T_C and T_S, by a power law relationship involving the fractional vegetation cover.

The second assumption is that the net radiation absorbed by the plant canopy, Rn_C, is partitioned between H_C and LE_C using the Priestley-Taylor approximation [35] to estimate LE_C, which can be over-ridden when the vegetation is stressed. An estimate of Rn_C is computed using *LAI* and assuming that the extinction of *Rn* inside the canopy layer can be approximated using Beer's Law [36], namely,

$$Rn_C = Rn\,(1 - \exp(-\beta\, LAI)) \qquad (10)$$

where the constant β is the extinction coefficient. A value of $\beta = 0.45$ is midway in the observed range (i.e. 0.3–0.6) for vegetation [36].

This approach was evaluated with data available from the Monsoon 90 experiment conducted over the arid Walnut Gulch watershed in Arizona, *figure 7*, during the summer (Monsoon season) of 1990 [25]. Data from a Landsat 5 TM scene of September 1990 were used to develop the land-use map for the four categories present in the watershed and the spatial variation of NDVI and thus LAI. The land-use map was used to set the roughness parameters for the different surface characteristics: grass, shrub, etc.

The thermal infrared data used are from channel 8 of the NS001 sensor on board the NASA C-130 aircraft and are shown in *figure 8* for 3 days during the experiment, days 213, 216 and 221. The bandpass for this channel is approximately 10–12 µm.

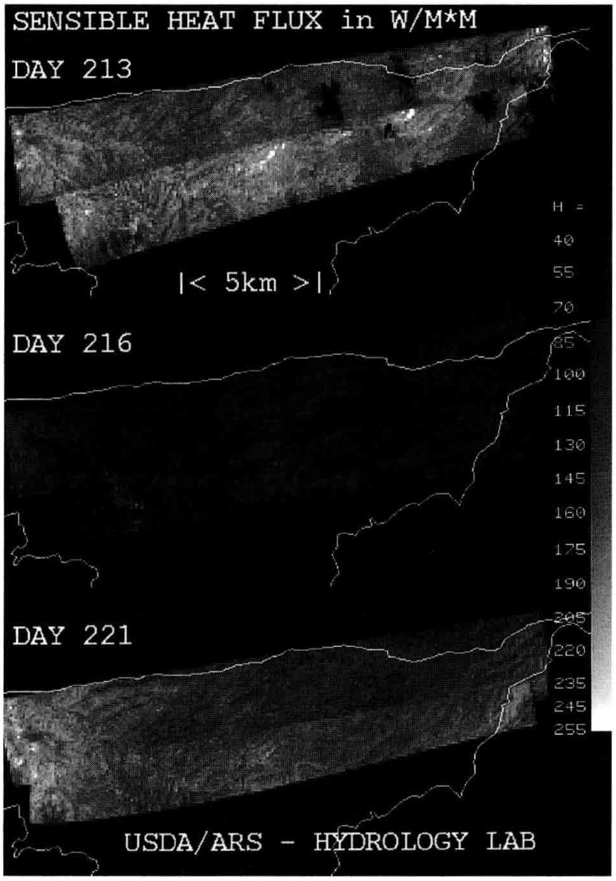

Figure 9. The spatial variation of the surface sensible heat flux derived from surface temperatures given in *figure 8* but degraded to a spatial resolution of 90 m for the 3 days.

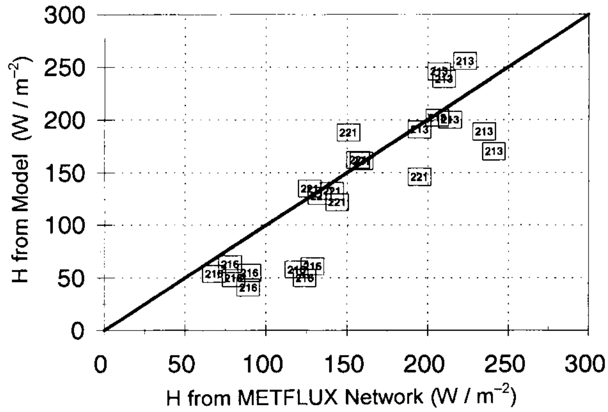

Figure 10. Comparison of estimated sensible heat flux with the ground observations for the eight METFLUX stations. The remotely sensed values are the averages for a 3 × 3 pixel (270 × 270 m) area around each station.

The data are from two flight lines at an altitude of 2 400 m above ground, yielding a pixel size of about 6.3 m. The data from the two lines on each day were merged to cover an area of about 6 by 20 km. The data were acquired at between 10:00 and 10:30 local time. The temperatures were corrected for atmospheric effects with Lowtran-7 using radiosondes launched at the site. The results of this correction process were compared with ground radiometer measurements and found to agree within 1 K [20]. The data for the 3 days show a range of conditions. The air temperatures were relatively consistent for the 3 days, about 25 °C, while the surface temperatures show considerable variation resulting from differences in the soil moisture status for the 3 days. Conditions were very dry on day 213 (1 August 1990, $< T_{surf} >$ = 37 °C) and quite wet on day 216 (4 August 1990, $< T_{surf} >$ = 31 °C) following up to 50 mm of rain on the previous 3 days. Note the narrow range of T_{surf} on this day. There were intermediate, and more variable, moisture conditions on day 221 (9 August 1990, $< T_{surf} >$ = 33 °C).

These maps of surface temperature were used in the model discussed in section 2.1 to determine the heat fluxes over the study area on the 3 days. The results for the sensible heat flux are shown in *figure 9*, which as expected, show that the sensible heat flux was highest on day 213 and lowest on day 216. Comparisons of the values estimated from the model and the ground observations at the eight METFLUX sites are presented in *figure 10*. The results show a good linear relation between the two with r^2 = 0.8. It is clear, however, that on the wet day, 216, the model is not predicting the same level variation as that observed on the ground. Apparently the model is over predicting either the ground heat flux or the latent heat flux which is resulting in reduced sensible heat fluxes. Recent improvements to the model parameterizations have been made. These include a more physically based algorithm for the extinction of R_n inside the canopy layer, a more robust formulation for R_s and a new algorithm which allows for a variable Priestly-Taylor α parameter [26].

4. DISCUSSION

The results of Salisbury and D'Aria [38] indicate that a detailed analysis of emissivity spectra for soils may yield information on the soil texture (particle sizes), organic content and/or moisture content. While these properties are detectable in laboratory spectra it remains to be seen if they will be observable from a remote platform such as the aircraft instrument with a small number of bands, e.g. the TIMS or the advance spaceborne thermal emission and reflection (ASTER) Radiometer to be flown on the EOS-AM spacecraft in 1999 [51]. The variation of bare soil emissivity with wavelength, λ, indicates that care must be taken in using broadband infrared radiometer results to infer surface temperature. The results for vegetated canopies, i.e. emissivity ≈ 1 with little or no spectral variation, are very encouraging for the possible use of split window approaches for eliminating atmospheric effects in thermal infrared determinations of surface temperatures of vegetation.

In this paper we have reviewed the physics of the energy balance at the land surface and the factors that can be accessed through remote sensing. These include the incoming solar radiation, R_s, the surface albedo, α, and vegetation indices from the VNIR channels of ASTER. The longwave radiation components, $R_{L\downarrow}$ and $\varepsilon\sigma T^4$, can be estimated from temperature sounding instruments and from surface temperature observations. The primary contribution that ASTER can make to surface flux determinations will be through the thermal infrared channels. The problems with estimating the sensible heat flux were discussed and an example from the Monsoon 90 experiment was presented. In this case we used Landsat TM data to simulate the ASTER VNIR data and aircraft thermal infrared to simulate the ASTER thermal infrared data. These data were incorporated into a two-source model to estimate sensible heat flux by taking into account spatial variations in the vegetation and land-use patterns. Up until now this approach has been tested on only sparse or limited vegetation conditions. We are currently working on extending the approach to other areas for which we have remotely sensed surface temperature data.

REFERENCES

[1] André J.C., Goutorbe J.P., Perrier A., Becker F., Bessemoulin P., Bougeault P., Brunet Y., Brutsaert W., Carlson T., Cuenca R., Gash J., Gelpe J., Hildebrand P., Lagouarde J.P., Lloyd C., Mahrt L., Mascart P., Mazaudier C., Noilhan J., Ottlé C., Payen M., Phulpin T., Stull R., Shuttleworth J., Schmugge T., Taconet O., Tarrieu C., Thepenier R.M., Valencogne C., Vidal-Madjar D., Weill A., Evaporation over land surfaces: First results from HAPEX-MOBILHY special observing period, Ann. Geophys. 6 (1988) 477–492.

[2] Bartholomew M.J., Kahle A.B., Hoover G., Infrared spectroscopy (2.3–20 ·mm) for the geological interpretation of remotely sensed multispectral thermal infrared data, Int. J. Remote Sensing 10 (1989) 529–544.

[3] Bastiaanssen W.G.M., Menenti M., Feddes R.A., Holtslag A.A.M., A remote sensing surface energy balance algorithm for land (SEBAL) 1. Formulation, J. Hydrol. 212–213 (1998) 198–212.

[4] Bastiaanssen W.G.M.,Pelgrum H., Wang Y., Ma Y., Moreno J.F., Roerink G.J., van der Wal T., A remote Sensing surface energy balance algorithm for land (SEBAL) 2. Validation, J. Hydrol. 212–213 (1998) 213–229.

[5] Becker F., The impact of spectral emissivity on the measurements of land surface temperature from a satellite, Int. J. Remote Sensing 8 (1987) 1509–1522.

[6] Becker F., Li Z-L., Towards a local split window over land surfaces, Int. J. Remote Sensing 11 (1990) 369–393.

[7] Berk A., Bernstein L.S., Anderson G.P., Acharya P.K., Robertson D.C., Chetwynd J.H., Adler-Golden S.M., MODTRAN cloud and multiple scattering upgrade with application to AVIRI, Remote Sensing Environ. 65 (1998) 367–375.

[8] Breon F.-M., Frouin R., Gautier C., Satellite estimates of downwelling longwave irradiance at the zurface during FIFE, Proc. Am.Meteorol. Soc. Symp. on the First ISLSCP Field Experiment (FIFE), 7–9 February, 1990, Anaheim, CA, Am. Meteorol. Soc., Boston, MA, 1990, pp. 92–97.

[9] Brutsaert W., On a derivable formula for longwave radiation from clear skies, Water Resour. Res. 11 (1975) 742–744.

[10] Camillo P.J., Gurney R.J., Schmugge T.J., A soil and atmospheric boundary layer model for evapotranspiration and soil moisture studies, Water Resources Res. 19 (1983) 371–380.

[11] Camillo P.J., Using one- or two-layer models for evaporation estimation with remotely sensed data, in: Schmugge T.J., Andre J.-C. (Eds.), Land Surface Evaporation: Measurement and Parameterization, Springer-Verlag New York Inc., 1991, pp. 183–197.

[12] Carlson T.N., Regional scale estimates of surface moisture availability and thermal inertia using remote thermal measurements, Remote Sensing Rev. 1 (1986) 197–247.

[13] Carlson T.N., Buffum M.J., On estimating total daily evapotranspiration from remote surface temperature measurements, Remote Sensing Environ. 29 (1989) 197–207.

[14] Dedieu G., Deschamps P.Y., Kerr Y.H., Satellite estimation of solar irradiance at the surface of the earth and of surface albedo using a physical model applied to Meteosat data, J. Climatol. Appl. Meteorol. 26 (1987) 79–87.

[15] Diak G., Gautier C., Improvements to a simple model for estimating insolation from GOES data, J. Climatol. Appl. Meteorol. 22 (1983) 505–508.

[16] Gillespie A., Rokugawa S., Matsunaga T., Cothern J.S., Hook S., Kahle A.B., A temperature and emissivity separation algorithm for advanced spaceborne thermal emission and reflection radiometer (ASTER) images, IEEE Trans. Geosci. Remote Sensing 36 (1998) 1113–1126.

[17] Grassl H., Extraction of surface temperature from satellite data, in: Toselli F. (Ed.), Applications of Remote Sensing to Agrometeorology, Kluwer Academic Publ., 1989, pp. 199–220.

[18] Hall F.G., Huemmrich K.F., Goetz S.J., Sellers P.J., Nickeson J.E., Satellite remote sensing of qurface energy balance: success, failures and unresolved issues in FIFE, J. Geophys. Res. 97 (1992) 19061–19089.

[19] Huband N.D.S., Monteith J.L., Radiative surface temperature and energy balance of a wheat canopy: I. Comparison of radiative and aerodynamic canopy temperatures, Boundary Layer Meteorol. 36 (1986.) 1–17.

[20] Humes K.S., Kustas W.P., Goodrich D.C., Spatially distributed sensible heat flux over a semi-arid watershed. Part 1: Use of radiometric surface temperature and a spatially uniform resistance, J. Appl. Meteorol. 36 (1997) 281–292.

[21] Jackson R.D., Reginato R.J., Idso S.B., Wheat canopy temperature: a practical tool for evaluation water requirements, Water Resources Res. 13 (1977) 651–656.

[22] Kahle A.B., Alley R.E., Separation of temperature and emittance in remotely sensed radiance measurements, Remote Sensing Environ. 42 (1992) 107–112.

[23] Kerr Y.H., Lagouarde J.-P., Imbernon J., Accurate land surface temperature retrieval from AVHRR data with use of an improved split window algorithm, Remote Sensing Environ. 41 (1992) 197–209.

[24] Kustas W.P., Daughtry C.S.T., Estimation of the soil heat flux/net radiation ratio from spectral ata, Agric. For. Meteorol. 49 (1990) 205–223.

[25] Kustas W.P., Goodrich D.C., Preface: Special issue on the Monsoon'90 multi-disciplinary experiment, Water Resources Res. 30 (1994) 1211–1225.

[26] Kustas W.P., Norman, J.M., Schmugge, T.J., Anderson M.C., Mapping surface energy fluxes with radiometric temperature, in: Quattrochi D., Luvall J. (Eds.), Thermal Remote Sensing in Land Surface Processes, Ann Arbor Press, Ann Arbor, MI, USA, 1999 (in press).

[27] McClain E.P., Pichel, W.G., Walton C.C., Ahmed Z., Sutton J., Multichannel improvements to satellite derived global sea surface temperatures, Adv. Space Res. 2 (1983) 23–47.

[28] Nerry F., Stoll M.P., Pion J.C., Infrared spectroradiometry, in: Kerr Y.H., Mahkmara H., Meunier J.C.,Valero T., HAPEX SAHEL Ground data version 4, CD–ROM 3, HSIS LERTS/CNES/ORSTOM, distributed by MEDIAS–FRANCE, Toulouse, France, 1997.

[29] Norman J.M., Chen J., Goel N., Thermal emissivity and infrared temperature dependency of plant canopy architecture and view angle, Proc. IEEE Int. Geoscience and Remote Sensing Symp. (IGARSS'90), 2–24 May 1990, College Park, Maryland, vol. III, 1990, pp. 1747–1750.

[30] Norman J.M., Divakarla M., Goel N.S., Algorithms for extracting information from remote thermal-IR observations of the earth's surface, Remote Sensing Environ. 51 (1995) 157–168.

[31] Norman J.M., Kustas W.P., Humes K.S., A two-source approach for estimating soil and vegetation energy fluxes from observations of directional radiometric surface temperature, J. Agric. For. Meteorol. 77 (1995) 263–293.

[32] Palluconi F., Kahle A.B., Hoover G., Conel J.E., The spectral emissivity of prairie and pasture grasses at Konza Prairie, Kansas. Symp. on FIFE, Am. Meteorol. Soc., Boston, MA, 1990, pp. 77–78.

[33] Pelgrum H., Bastiaanssen W.G.M., An intercomparison of techniques to determine the area-averaged latent heat flux from individual in situ observations: A remote sensing approach using the European field experiment in a desertification–threatened area data, Water Resour. Res. 32 (1996) 2775–2786.

[34] Price J.C., The potential of remotely sensed thermal infrared data to infer surface soil moisture and evaporation, Water Resour. Res. 16 (1980) 787–795.

[35] Priestley C.H.B., Taylor R.J., On the assessment of surface heat flux and evaporation using large-scale parameters, Mon. Weather Rev. 100 (1972) 81–92.

[36] Ross J., The radiation regime and architecture of plants, in: Lieth H. (Ed.), Tasks for Vegetation Sciences, Vol. 3, Dr. W. Junk, The Hague, The Netherlands, 1981.

[37] Salisbury J.W., D'Aria D.M., Emissivity of terrestrial materials in the 8–14 μm atmospheric window, Remote Sensing Environ. 42 (1992) 83–106.

[38] Salisbury J.W., D'Aria D.M., Infrared (8–14 μm) remote sensing of soil particle size, Remote Sensing Environ. 42 (1992) 157–165.

[39] Schmugge T., Hook S.J., Coll C., Recovering surface temperature and emissivity from thermal infrared multispectral data, Remote Sensing Environ. 65 (1998) 121–131.

[40] Schmugge T.J., Becker F., Li Z.-L., Spectral emissivity variations observed in airborne surface temperature measurements, Remote Sensing Environ. 35 (1991) 95–104.

[41] Seguin B., Itier B., Using midday surface temperature to estimate daily evaporation from satellite thermal IR data, Int. J. Remote Sensing 4 (1983) 371–383.

[42] Shanda E., Physical Fundamentals of Remote Sensing, Springer-Verlag, Berlin, 1986.

[43] Shuttleworth W.J., Evaporation models in hydrology, in: Schmugge T.J., Andre J.-C. (Eds.), Land Surface Evaporation: Measurement and Parameterization, Springer-Verlag New York, 1991, pp. 93–103.

[44] Soer G.J.R., Estimation of regional evapotranspiration and soil moisture conditions using remotely sensed crop surface temperatures, Remote Sensing Environ. 9 (1980) 27–45.

[45] Starks P.J., Norman J.M., Blad B.L., Walter-Shea E.A., Walthall C.L., Estimation of Shortwave Hemispherical Reflectance (Albedo) from bidirectionally reflected radiance data, Remote Sensing Environ. 38 (1991) 123–134.

[46] Stewart J.B., Kustas W.P., Humes K.S., Nichols W.D., Moran M.S., DeBruin H.A.R., Sensible heat flux - radiometric surface temperature relationship for semiarid areas, J. Appl. Meteor. 33 (1994) 1110–1117.

[47] Suttles J.T., Ohring G. (Eds.), Surface radiation budget for climate applications, NASA Ref. Pub. 1169, 1986.

[48] Taconet O., Bernard R., Vidal-Madjar D., Evapotranspiration over an agricultural region using a surface flux/temperature model based on NOAA AVHRR data, J. Clim. Appl. Meteorol. 25 (1986) 284–307.

[49] Wan Z., Dozier J., A generalized split-window algorithm for retrieving land-surface temperature for space, IEEE Trans. Geosci. Remote Sensing 34 (1996) 892–905.

[50] Wigneron J.-P., Schmugge T., Chanzy A., Calvet J.-C., Kerr Y., Use of passive microwave remote sensing to monitor soil moisture, Agronomie 18 (1998) 27–43.

[51] Yamaguchi Y., Kahle A.B., Tsu H., Kawakami T., Pniel M., Overview of advanced spaceborne thermal emission and reflection radiometer (ASTER), IEEE Trans. Geosci. Remote Sensing 36 (1998) 1062–1071.